CZECH TECHNICAL
UNIERSITY
IN PRAGUE

FACULTY
OF ELECTRICAL
ENGINEERING

BACHELOR THESIS

2022

JIMI
XU

CZECH TECHNICAL UNIVERSITY IN PRAGUE

Faculty of Electrical Engineering

Department of Physics

Bachelor Thesis:

Stability and aging of perovskite solar cell materials

Project of:	Jimi Xu
Supervisor:	Ing. Jaroslav Kuliček, Ph.D.
Study program:	Electrical Engineering and Computer Science

Prague 2022

BACHELOR'S THESIS ASSIGNMENT

I. Personal and study details

Student's name: **Xu Jimi** Personal ID number: **490382**

Faculty / Institute: **Faculty of Electrical Engineering**

Department / Institute: **Department of Physics**

Study program: **Electrical Engineering and Computer Science**

II. Bachelor's thesis details

Bachelor's thesis title in English:

Stability and aging of perovskite solar cell materials

Bachelor's thesis title in Czech:

Stabilita a stárnutí materiálů pro solární články na bázi perovskitů

Guidelines:

Perovskites are intensively studied materials for photovoltaic solar cells due to their high mobility of charge carriers and high tolerance to defects. Research of perovskite solar cells (PSCs) has made significant progress but there are still not fully understood defects along grain boundaries and interfaces that decisively affect the performance and stability of these devices.
1. Get acquainted with the recommended literature and overview the current state of the issue. Focus mainly on perovskite defects along grain boundaries and interfaces.
2. Use the Scanning Kelvin Probe method to measure the photovoltaic response under cold light lighting and the AM1.5 solar simulator for already prepared samples.
3. The optical properties and morphology of PSCs characterize by Confocal Photoluminescence and Atomic Force Microscopy.
4. Evaluate the measured results and discuss them with the published data.

Bibliography / sources:

[1] A. Abudulimu et al. J. Energy Chem. 47 (2020) 132-137, doi:10.1016/j.jechem.2019.12.002.
[2] J. Kuliček et al. Proc. of the NANOCON 2019, doi: 10.37904/nanocon.2019.8662.

Name and workplace of bachelor's thesis supervisor:

Ing. Jaroslav Kuliček, Ph.D. Department of Physics FEE

Name and workplace of second bachelor's thesis supervisor or consultant:

Date of bachelor's thesis assignment: **09.02.2022** Deadline for bachelor thesis submission: **20.05.2022**

Assignment valid until: **30.09.2023**

Ing. Jaroslav Kuliček, Ph.D.	prof. Ing. Ondřej Jiříček, CSc.	prof. Mgr. Petr Páta, Ph.D.
Supervisor's signature	Head of department's signature	Dean's signature

III. Assignment receipt

The student acknowledges that the bachelor's thesis is an individual work. The student must produce his thesis without the assistance of others, with the exception of provided consultations. Within the bachelor's thesis, the author must state the names of consultants and include a list of references.

. | Date of assignment receipt

Student's signature

Declaration:

I declare that the presented work was developed independently and that I have listed all sources of information used within it in accordance with the methodical instructions for observing the ethical principles in the preparation of university theses.

Prague, date ....

Author's signature

Acknowledgment:

I would like to express my deepest appreciation to my supervisor, Jaroslav Kuliček, for his invaluable patience and feedback.

Thanks should also go to my classmates for their ideas sharing, late-night feedback, and recommendation. I would like to extend my sincere thanks to my Physics professor, Bohuslav Rezek, for his advice and suggestions about the project. Therefore, I can find a topic that I am interested in.

Lastly, I would be remiss in not mentioning my family, especially my parents, who gave me lots of support and confidence, so I can finish the project without any worries. I would also like to thank my dog for all the entertainment and pressure relief.

Abstract

Perovskite (PVSK) solar cells have become the mainstream research in the past few years. They generate very good laboratory results in the conversion of energy. However, the problematic part of PVSK is its stability and sensitivity to the environment. In this thesis, we studied the degradation and aging of the PVSK with different ratios of MAI/PbI_2 and different combinations of the charge transporting layers (CTLs) after a period of two years. The ratios we used for MAI/PbI_2 were 0.9 and 1.0. Moreover, we used two types of CTLs, SnO_2 as the electron transporting layer and Spiro-OMeTAD as the hole transporting layer. The morphology of the samples was characterized by Atomic Force Microscopy. The spectra and mapping were measured by the Confocal Photoluminescence (PL) microspectroscopy. The surface potential and photovoltage were studied by Scanning Kelvin Probe in the dark and under illuminations. We used two sources of illumination, Solar Simulator and Halogen lamp. The Kelvin Probe studies illustrate that the samples with the ratio MAI/PbI_2=0.9 are less stable than the samples with the ratio of 1.0. The substrate ITO glass significantly influenced the photovoltage of the samples. PL maps show significant local variation of intensities and differences in the PL spectra. In spite of some degradation, perovskite samples are still photoactive after two years.

Key Words: Perovskite solar cells, photovoltage, degradation, charge-transporting layers, methylammonium, Kelvin Probe, Atomic Force Microscopy, Confocal Photoluminescence microspectroscopy

Table of contents

List of Abbreviations

PbI_2	Lead Iodide
SnO_2	Tin oxide
ITO	Indium Tin Oxides
$MAPbI_3$	Methylammonium lead oxide
CTL	Charge-transporting layers
MAI	Methylammonium
AFM	Atomic Force Microscopy
PVSK	Perovskite
PV	Photovoltage
PL	Photoluminescence spectroscopy
Spiro-OMeTAD	2,2',7,7'-Tetrakis[N,N-di(4-methoxyphenyl)amino]-9,9'-spirobifluorene
SKP	Scanning Kelvin Probe
TCO	Transparent Conducting Oxide
ETL	Electron Transporting layer
HTL	Hole Transporting layer

Figures

1. Introduction

Perovskite solar cells are solar cells that use perovskite-type organic metal halide semiconductors as light-absorbing materials [1–4]. They are the third generation of solar cells after crystalline silicon solar cells and thin-film solar cells. They have the advantages of simple structure, high photoelectric conversion efficiency, and low cost [3,5–7]. With the attention of many countries around the world, technical research is continuously deepening.

Perovskite (PVSK) materials are the core of perovskite solar cells. There are many types of perovskite materials, and researchers are developing new perovskite solar cells without lead iodide methylamine [8–11].

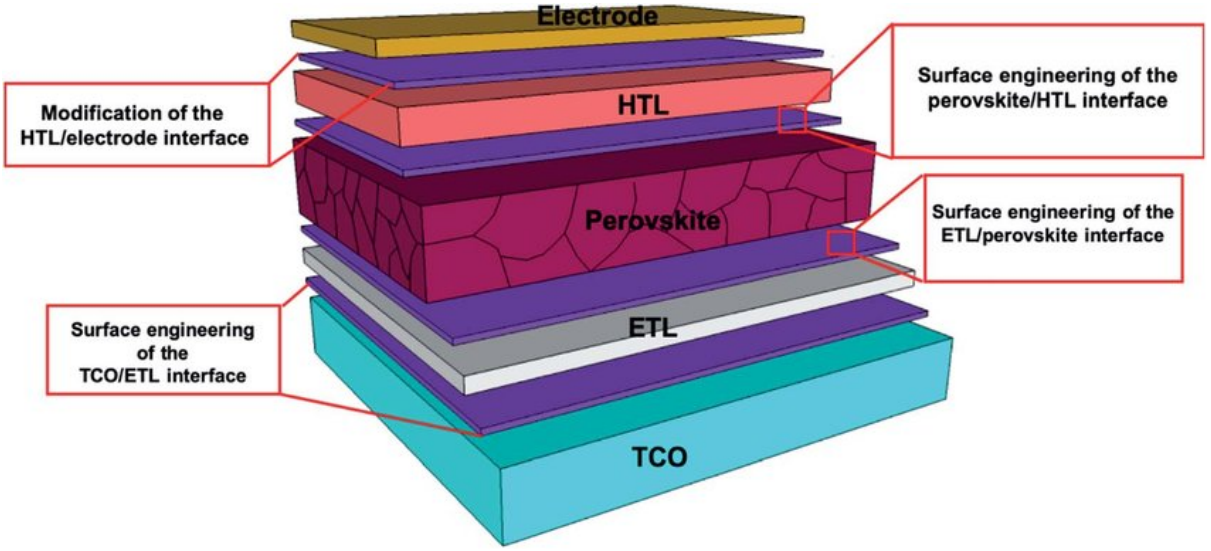

Fig. 1.1 Standard design of a perovskite solar cell [12].

Perovskite solar cell is designed as:

-TCO: often used ITO or FTO.

-ETL: often used SnO_2.

-Perovskite.

-HTL: often used Spiro-OMeTAD.

-Electrode: often used gold.

At this stage, monocrystalline silicon solar cells dominate the global market. After continuous development, the photoelectric conversion efficiency of monocrystalline silicon has approached the top, and further development is difficult. However, the performance requirements of solar cells in the photovoltaic power generation market are still increasing [13]. The photoelectric conversion

efficiency of perovskite materials is higher than that of monocrystalline silicon, and the theoretical limit can reach 33% [14,15]. In the future, if perovskite solar cells can replace monocrystalline silicon solar cells, the market development potential is huge.

Nevertheless, perovskite solar cells still have certain technical defects. For example, the structural stability of perovskite materials is insufficient, and the performance is easily degraded in harsh environments [16,17]. In addition, perovskite materials are difficult to deposit as thin films in large areas and perovskite solar cells generally contain metallic lead, which can cause harm to human health and the ecological environment [18,19]. Although there is already a lead-free perovskite solar cell in development [20], in this thesis we will be using solar cells with lead because it is a type of solar cell we used in the research 2 years ago. Furthermore, another significant shortcoming of PVSK material is the usage time. This material has a high speed of degradation, it is in stable use for 3 months or so, after this period it will become extremely unstable. The reason is the iodide-based perovskites will produce a gaseous form of iodine during operation, because of the relatively high vapor pressure of gaseous iodine, it can quickly permeate the rest of the perovskite material, causing damage to the whole solar cell [21]. This led to accelerated decomposition of the $MAPbI_3$ perovskite material into PbI_2. As a consequence, it causes degradation of perovskite [21]. In addition, there are also some other factors that lead to the perovskite solar cells' degradation faster, such as humidity [22], thermal stability [23], and ion migration [1,2]. Due to these characteristics, it can not compete with the solar cell in the current market, but researchers are working on the stability and environmental safety of perovskite materials because the energy conversion potential of perovskite is not overcome yet.

The stability of the perovskite solar cells has significance for commercial production. The researchers studied the influence of the hole transporting layer (HTL) and electron transporting layer (ETL) on ionic migration as well as the stability and aging of perovskite materials in publications [1,2]. Authors studied lead iodide (PbI_2) methylammonium (MAI) based perovskites in the different ratios of MAI/PbI_2. There were three different ratios of MAI/PbI_2: MAI/PbI_2 =1.1 [1], MAI/PbI_2 =1 [1,2] and MAI/PbI_2 =0.9 [2]. Spiro-OMeTAD was used as HTL and SnO_2 as ETL. The four samples were prepared on the ITO glass: ITO/PVSK, ITO/SnO_2/PVSK, ITO/PVSK/spiro, and ITO/SnO_2/PVSK/spiro.

The authors characterized sample morphology by Atomic Force Microscopy. The morphology results showed that both CTLs and MAI can influence the morphology of the samples. Furthermore, the samples with the SnO_2 component reduced the granularity and improved the perovskite uniformity. In addition, Spiro filled the rough surface rather than being conformal. ITO/SnO_2/PVSK/Spiro provided the best overall PVSK uniformity, and this was an important feature for homogeneous charge collection via CTLs and reducing degradation due to ion migration [1,2].

The electronic properties/surface potential were characterized by the Atomic Force Microscopy and Scanning Kelvin Probe. Measurements were done in the dark and under illumination

during the time period [1,2]. Using the Kelvin Probe device could help researchers to better understand the influence of different ratios of MAI/PbI_2 to charge transporting layers and sample stability. In addition, the stability of samples in the time period was measured by SKP in the work of Kuliček et. al. [2]. The researchers measured samples as initial then after the 14th days and 28th days. Initial means that samples were taken from vacuum boxes stored in the dark.

The authors showed the sample ITO/PVSK with a ratio of MAI/PbI_2 = 0.9 was stable with work function (4.96 ± 0.03) eV [2] in the dark for the whole period of 28 days, the photovoltage was negative also remained stable after 28 days. The negative PV means that electrons were not extracted to the bottom electrode but rather diffused to the perovskite surface. Furthermore, the work function of sample ITO/PVSK/Spiro also remained stable at (5.28 ± 0.02) eV, there was not a significant change after 28 days [2]. Nevertheless, the photovoltage response was slightly different after 28 days. The authors showed that the HTL spiro was actually able to extract some holes to the surface. Also, researchers displayed that sample ITO/PVSK/SnO_2 had a lower work function compared to ITO/PVSK and observed some persistent charging during the dark-light cycle as well as fluctuation in the work function between (4.73 ± 0.06) eV and (4.54 ± 0.06) eV [2] during the dark. The last sample, ITO/SnO_2/PVSK/Spiro showed a decrease in work function during the dark measurement and positive PV [2].

The samples with the ratio of MAI/PbI_2 = 1.0 were also analyzed in the article [2]. The authors showed decreasing in the work function in the dark measurement for ITO/PVSK sample. Therefore, the photovoltage fluctuated during the 28 days. The ITO/PVSK/Spiro sample was stable for 14 days and decreased after 28 days. However, the photovoltage response was higher and positive. The work function, as well as the photovoltage of the sample ITO/SnO_2/PVSK, fluctuated during 28 days. In addition, for the ITO/SnO_2/PVSK/spiro sample with complete layers, the work function in dark decreased from (5.26 ± 0.06) to (5.02 ± 0.06) eV during 28 days. However, the photovoltage also remained positive in this case [2]. The article [1,2] showed that the same CTLs had slower kinetics and photovoltage fluctuated during the dark-light cycle. These effects of excess MAI are most likely due to the effects of ion migration.

The influence of CTLs on the ion migration in the perovskite solar cells was also studied in Photoluminescence (PL) by Abudulimu et al. [1]. The authors showed that the CTLs could create local charges and recombination processes with a minimum ion migration effect.

The motivation for this work is to investigate and characterize how aging of the perovskite samples stored in a dark place under environmental conditions can affect the morphology, photovoltaic, and optical properties.

In this thesis, we study the samples prepared by using precursor stoichiometry (methylammonium (MAI) and PbI_2) in two different ratios MAI/PbI_2 =1.0 and MAI/PbI_2 =0.9. As charge-transporting layers, Spiro-OMeTAD is used as HTL, and SnO_2 is used as ETL. We use the same samples as in the article [2] but two years later. The degradation processes of $MAPbI_3$ perovskite

during the storage time is the focus of this work. Using the Scanning Kelvin Probe, we measure the influence of CTLs and the different ratios of MAI and PbI_2. Two years ago, the surface potential of the perovskite samples was measured under the light from a Halogen lamp. In addition, we use a new type of light source Solar Simulator which is not used in the previous analysis. We compare results obtained from the two different sources of light. In addition, Atomic Force Microscopy and Confocal Photoluminescence are used to obtain the samples optical images, morphology, PL spectra, and PL maps. Obtained data are analyzed and give us more information on the current state of the samples. Furthermore, the influence of CTLs and MAI on the perovskite properties is described.

2. Experimental

2.1 Sample preparation

The ITO substrates were cleaned with isopropanol and distilled water in the ultrasonic bath before SnO_2 was spin-coated. Spin-coated SnO_2 was annealed at 150 °C for 20 minutes in ambient. PbI_2 (dissolved in the DMF) was spin-coated onto substrate ITO/SnO_2 at 3000 rpm for 35s and the sample was annealed again. After, the MAI dissolved in 2-propanol was spin-coated and annealed at 100 °C for 30 minutes. Spiro-OMeTAD dissolved in a mixture of solutions was spin-coated onto an active layer at 3000 rpm for the 30s. Detailed sample preparation was described in [1].

2.2 Scanning Kelvin Probe

The Scanning Kelvin Probe is a non-contact device that measures the work function between a conducting specimen and a vibrating tip. The Kelvin method is an indirect technique, i.e. electrons are not extracted directly from the surface, instead of using a reference surface (a vibrating tip) as the counter electrode the surface under study forms one plate of a parallel plate capacitor. Electrons flow back and forth in the external circuit as the tip vibrates. The work function difference is determined by the addition of an external voltage, termed the backing potential (Vb) [24]. The Scanning Kelvin Probe in the glove box from KP Technology is shown in Fig. 2.1.

A) B)

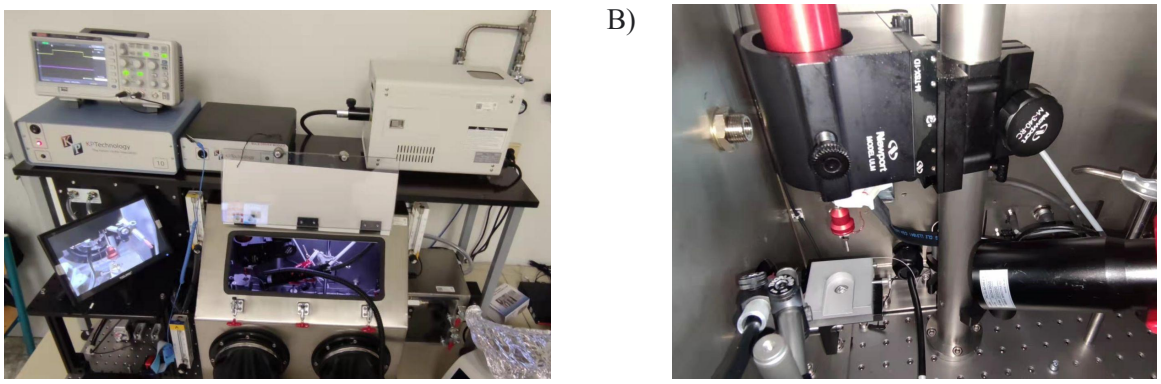

Fig. 2.1 A) Glove box with Kelvin probe, B) Kelvin Probe in the glove box.

2.2.1 Measurement settings

Before we started with the experiment, we needed to measure a gold sample as a control variable for the calculation of the work function. Samples were measured by the Kelvin Probe in the glove box (see Fig. 2.1 and Fig. 2.2) by using the software of RHC040 v12.07 from KP technology. Before we started with the measurement we needed to set a gradient of 300 by adjusting the distance between the sample and the vibrating tip, so the distance will be controllable to ensure the accuracy of the data. The gradient of 300 was set for every measured sample. We did a 300-point control measurement for the WF. Subsequently, we measured 1500 points of WF, and at every 300 points, the illumination was switched on. We created the dark-light-dark-light-dark cycle. The samples were illuminated by the halogen lamp and the solar simulator. We used the light intensity of 1.5AM for the solar simulator and standard light intensity for the halogen lamp. Obtained potential namely contact potential difference was calculated to Work Function (WF) in eV. The equation is below:

$$WF_{sample} = (CPD_{sample} - CPD_{ref}) \times 10^{-3} + WF_{ref} \quad (1)$$

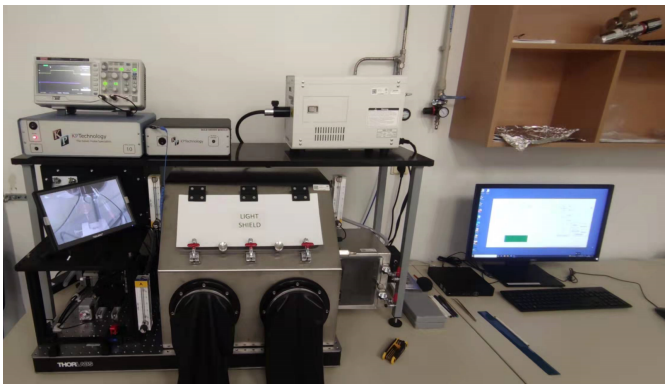

Fig. 2.2 Workspace with Kelvin Probe device.

2.3. Atomic Force Microscopy

Atomic Force Microscopy (AFM) is an analytical instrument that can be used to study the surface structure of solid materials, including insulators. It traces the topography of samples with extremely high - up to atomic - resolution by recording the interaction forces between the surface and a sharp tip mounted on a cantilever [25]. AFM provides spatial information parallel and perpendicular to the surface. In addition to high-resolution topographic information, local material properties such as adhesion and stiffness can be investigated by analyzing tip-sample interaction forces. The device type used in this thesis is WITec alpha300 RAS (see Fig. 2.3).

The software Control Five 5.2 was used for the collection of data and software Project Five 5.2 was used for data evaluation. Budget Sensors tips Multi 75Al-G with frequency 75 kHz and spring constant 3 N/m were used for data collecting. Firstly, we scan the larger area of 25x25 μm and then choose the smaller area of 5x5 μm, the set point was 0.25 V, and the scan speed was 2.56 line/s. Observed data gave more information about sample morphology, grain size, and roughness.

A)

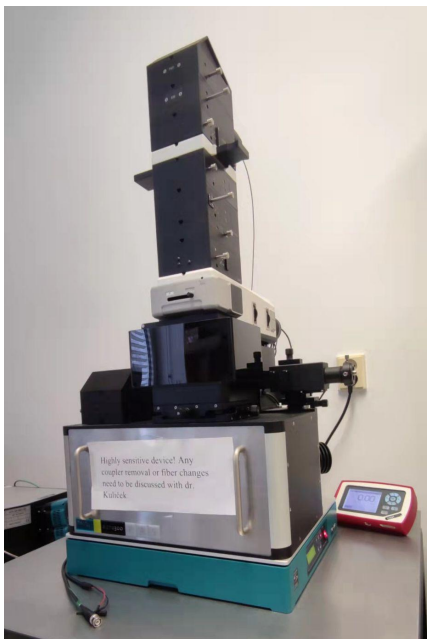

B)

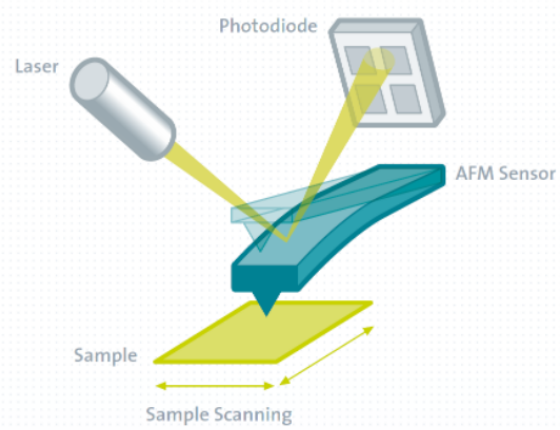

Fig. 2.3 A) AFM device in laboratory, B) working principle of AFM [25].

2.3 Halogen Lamp

The following figure illustrates the Halogen lamp, KL 1500 HAL, it is intended for industrial and laboratory applications. Cold light sources are used for the intensive illuminations of all types of objects. The infrared portions of the lamp's radiation are filtered out. Halogen lamps emit high-intensity visible light. As light absorbing materials have the physical property of converting incident light into heat. It has an illumination of 450 L/rad [26].

Fig. 2.4 Schott KL 1500 Halogen lamp wavelength range – visible light, 380-750 nm.

2.4 Solar Simulator

The basic principle of the solar simulator is to emit simulated solar light by the actions of a xenon lamp and proprietary air mass filter. We used Solar Simulator HAL - C100 (Asahi Spectra Co., Ltd.). Fig. 2.5 shows a Solar simulator.

Fig. 2.5 Solar Simulator HAL - C100 wavelength range 400-1100 nm.

2.5 Photoluminescence spectroscopy

Photoluminescence spectroscopy, often abbreviated as PL, is a form of light emission spectroscopy in which the light emission comes from a process called photo-excitation. During the excitation, the electrons within the materials move into excitement as the light shines onto the sample. The energy will release in the form of light when the electrons relax from the excited states to their equilibrium, known as relaxation [27]. In this thesis, PL spectra and maps were measured by system WITec alpha300 RAS using the confocal microscope-connected CCD detector (see Fig. 2.6). A supercontinuum laser was used for light excitation with an excitation wavelength of 532 nm. Filter 570 nm was put before the detector to filter laser light. We used the lens with a magnification of 50x to collect the spectra and PL maps in the range of 5x5 μm.

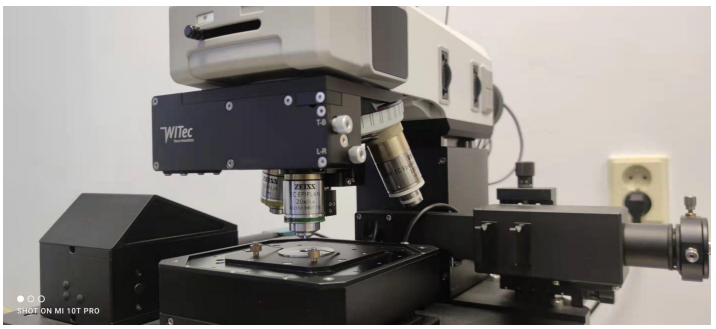

Fig. 2.6 The lens of WITec alpha 300 RAS device.

3. Results and discussion

3.1 Optical and Atomic Force Microscopy characterization

For the following two figures, Fig. 3.1 and Fig. 3.2 are the sample pictures, the optical images recorded by optical microscope, and AFM morphology images of the sample. Fig. 3.1 shows the ratio of 0.9 for MAI/PbI_2 and Fig. 3.2 shows the ratio of 1.0 for MAI/PbI_2. Each column represents one type of perovskite solar cells with different CTL, which are ITO/PVSK, ITO/SnO_2/PVSK, ITO/PVSK/Spiro, and ITO/SnO_2/PVSK/Spiro.

Observing the sample photographs(first row) from Fig. 3.1 and Fig. 3.2, we can clearly see the differences between the pictures. The pictures from ITO/PVSK/Spiro and ITO/SnO_2/PVSK/Spiro are more transparent than the others. Especially the pictures in Fig. 3.1, it may be due to the fact that there is less MAI. The transparent samples made an impact on our data collection work, and we had to slightly change the parameters for the data collection of these two samples but generally we needed to change parameters for all samples. We needed data collected with the same conditions. Thus, we needed to use an objective with resolution 50x for PL measurement because we could not find a focus by objective with resolution 100x. In the article Abudulimu et al. [1] for all PL measurements were used objective with resolution 100x.

Looking at the optical images recorded by optical microscopy images in Fig. 3.1, it has huge changes after two years of period, we can notice that the image of ITO/PVSK shows a light green surface with some red lines, they might be scratches and they can be also observed on the sample photographs. Nevertheless, the image of ITO/PVSK two years ago had a darker green surface, so the color of the surface has “faded”. Then, in the second image ITO/SnO_2/PVSK the color changes from green to light brown after adding SnO_2, and there are also some scratches with a black color. This is absolutely different compared with the image two years ago, the color changes from the light green. After the deposition of Spiro to the last two images, it is obvious that the surface changes to golden yellow. However, ITO/PVSK/Spiro looks darker than the full CTLs perovskite sample. We can also observe some occasional black spots on these two samples’ surfaces. It illustrates a different image in ITO/PVSK/Spiro two years ago, it illustrated crystal structures, but it has disappeared after two years. On the other hand, there are not many changes in the sample of ITO/SnO_2/PVSK/Spiro, just the color becomes lighter. It illustrates a different image in Fig. 3.2, the image of ITO/PVSK gives us a brown overview, but it had a cyan color two years ago. With the deposition of SnO_2 on the ITO surface the color changes to silver, it did not change to the color of light cyan as two years ago. They have a similar structure as the images two years ago after the addition of Spiro in Fig. 3.2. Both images illustrate a golden yellow surface, just the sample of ITO/PVSK/Spiro has turned from a greener

surface to a yellower surface. According the optical images we can conclude that there was some changes in the samples during the storage time.

In the AFM morphology images, we can see that after adding SnO_2 into ITO/PVSK the density of the grains is much higher and improves PVSK uniformity. This is also illustrated in the image of ITO/SnO_2/PVSK/Spiro, the density is higher after adding SnO_2 into ITO/PVSK/Spiro. One more fact, the surface roughness (Sq) of the samples decreases significantly after the Spiro coating. We measured the roughness of the grains in Fig. 3.1, they are 10.3 nm, 14.9 nm, 5.4 nm 6.7 nm respectively. As we can see the results in ITO/PVSK/Spiro and ITO/SnO_2/PVSK/Spiro have a much lower result than the sample without Spiro. This can be also seen in Fig. 3.2, the results still show a downward trend, even though the third data is slightly higher, which are 23.9 nm, 22.8 nm, 12.8 nm, and 9.1 nm, respectively. Moreover, if we compare the results of these two figures with different MAI/PbI_2 ratio, Fig. 3.1(MAI/PbI_2=0.9) and Fig. 3.2 (MAI/PbI_2=1.0), we can see the size of the grains in Fig. 3.2 are bigger than the grains in Fig. 3.1. For instance, the height and diameter of ITO/PVSK in Fig. 3.2 are 8.2 and 1091 nm whereas the height and the diameter of ITO/PVSK in Fig. 3.2 are 34.4 nm and 1729 nm. After two years the roughness changed. There is a decrease of the Sq values compared to the work of Kuliček et. al [2].

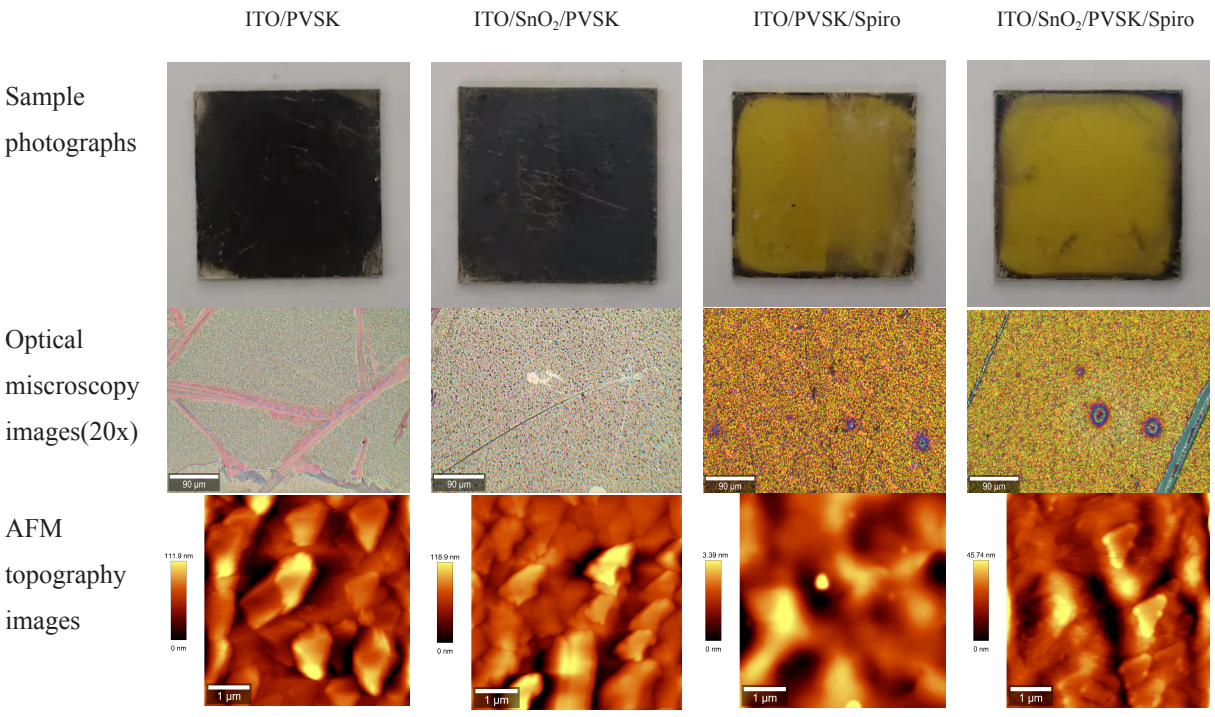

Fig. 3.1 Sample photographs, optical microscopy and AFM topography images for MAI/PbI_2=0.9.

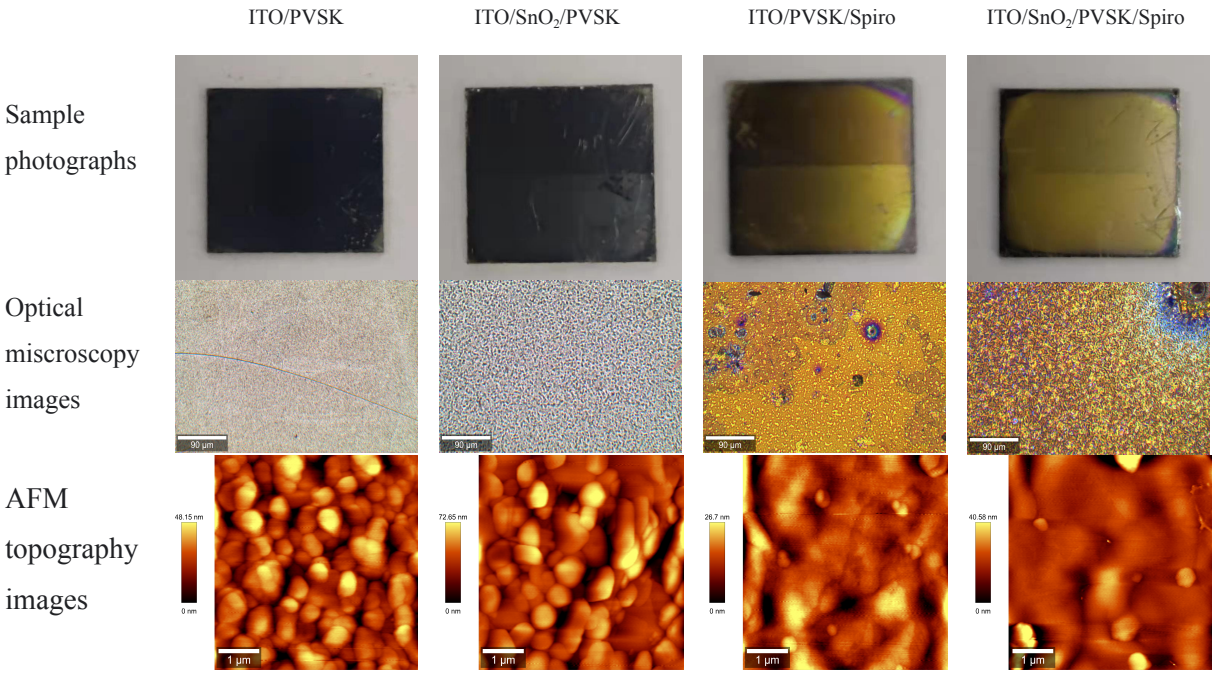

Fig. 3.2 Sample photographs, optical microscopy and AFM topography images for MAI/PbI_2=1.0.

3.2 Photoluminescence characterization

Fig. 3.3 illustrates the PL map with zoomed optical images for PVSK samples with a ratio of MAI/PbI_2=0.9. In the first row are the optical images and in the second row are the averaged PL maps with and without CTLs. For a better comparison of the PL maps, we used the averaging in the percentage. All the PL maps were recorded in the maximum intensity wavelength and full-width-half-maximum (FWHM) 40 nm. Optical images were described above in chapter 3.1. The average PL maps showed significant local intensities (red spots) probably related to PVSK features. Additionally we can see the similarities between the PL maps with the hole transporting layer, ITO/PVSK/Spiro and ITO/SnO_2/PVSK/Spiro.

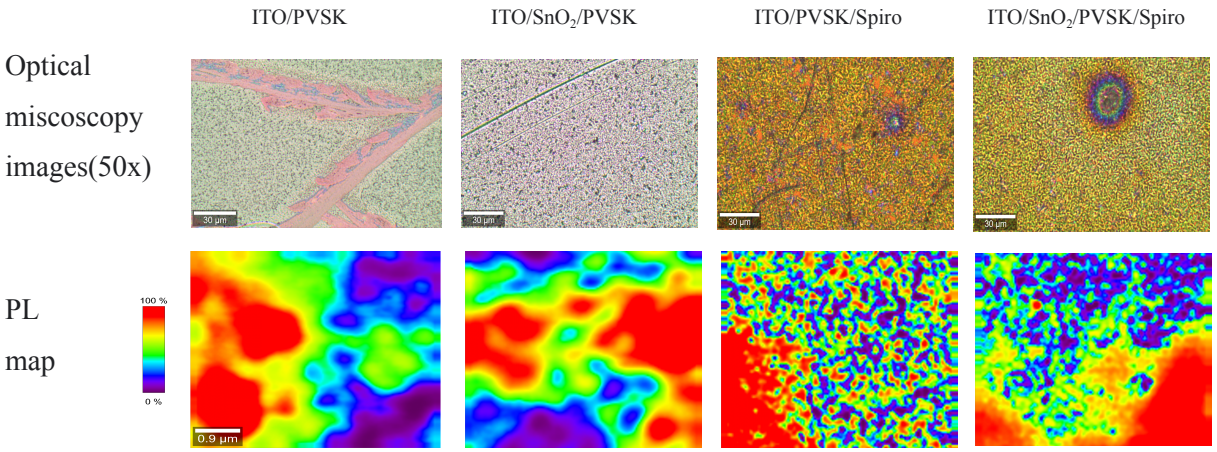

Fig 3.3 Optical microscopy images and PL map for MAI/PbI_2=0.9.

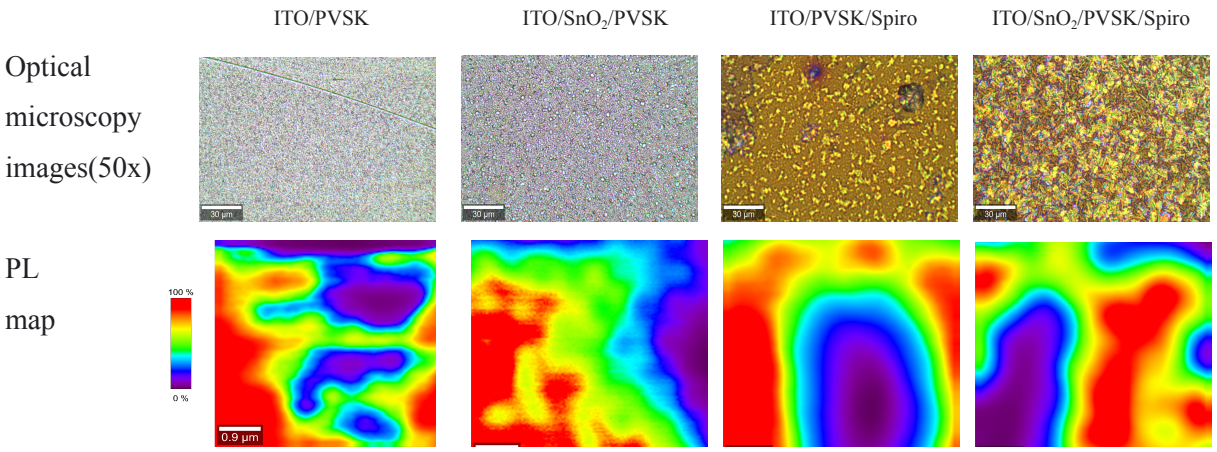

Fig. 3.4 Optical microscopy images and PL map for MAI/PbI_2=1.0.

Fig. 3.4 shows the optical images and averaged PL maps for perovskite samples with and without the charge transporting layers of MAI/PbI_2=1.0. Again, the optical images illustrated in the first row were discussed in chapter 3.1. In the second row, we can see the PL maps with the different spatial PL intensity variations. Different PL intensity variations could be related to the local differences in the charge generations and recombinations [1]. The PL maps have more similarities in the structure than the PL maps in Fig. 3.3. There are differences in the PL maps for samples ITO/PVSK/Spiro and ITO/SnO_2/PVSK/Spiro with ratio of MAI/PbI_2=0.9 and MAI/PbI_2=1.0. The PL features for MAI/PbI_2=0.9 become smaller for samples ITO/PVSK/Spiro and ITO/SnO_2/PVSK/Spiro. Opposite for MAI/PbI_2=1.0 where features become bigger. It seems that PL maps correlated with AFM maps. Thus relates to PVSK grain size. Although, we did not measure AFM maps and the PL maps in the same spots. The PL maps illustrate the charge recombination profile in the sample and formation of charge recombination profile gradients reflected ion migration [1]. Ion migration could affect the PVSK degradation [17]. The sample ITO/SnO_2/PVSK for the ratio MAI/PbI_2=1.0 illustrated small gradient and the small gradient were also observed for the ITO/SnO_2/PVSK for ratio of the

MAI/PbI_2=1.0 in the work of Abudulimu et. al. [1]. Also the PL features for the ratio of MAI/PbI_2=1.0 in the work of Abudulimu et. al. [1] are smaller the the PL features presented in this thesis. Two years old PL data are not available for the ratio of the MAI/PbI_2=0.9.

Fig. 3.5 illustrates the normalized PL spectra of perovskite samples with and without the CTLs. Fig. 3.5A shows normalized PL spectra for perovskite samples with the ratio of MAI/PbI_2=0.9. The spectra observed the highest intensity peaks in the wavelength range 760-767 nm. The spectra for samples with the Spiro hole transporting layer are unstable and left-shifted compared to the other two samples. The spectra shift could be related to the changes of the samples because these samples became most transparent in the two years.

The PL spectra with and without CTLs and the ratio of MAI/PbI_2=1.0 are shown in Fig. 3.5B. Again, spectra are normalized and observed; the highest intensity peak position of 767 nm is for samples ITO/PVSK, ITO/SnO_2/PVSK. The highest intensity peak position of 765 nm is for samples ITO/PVSK/Spiro and ITO/SnO_2/PVSK/Spiro. Again, there is a small left-shift for samples with the Spiro layer compared to the other two samples. Generally, the quality of the PL spectra for samples with MAI/PbI_2=1.0 were not significantly influenced by the layer stack while samples ITO/PVSK/Spiro and ITO/SnO_2/PVSK/Spiro with ration MAI/PbI_2=0.9 are influenced much more but PL spectra shifts also could be related to the transparency of the these samples.

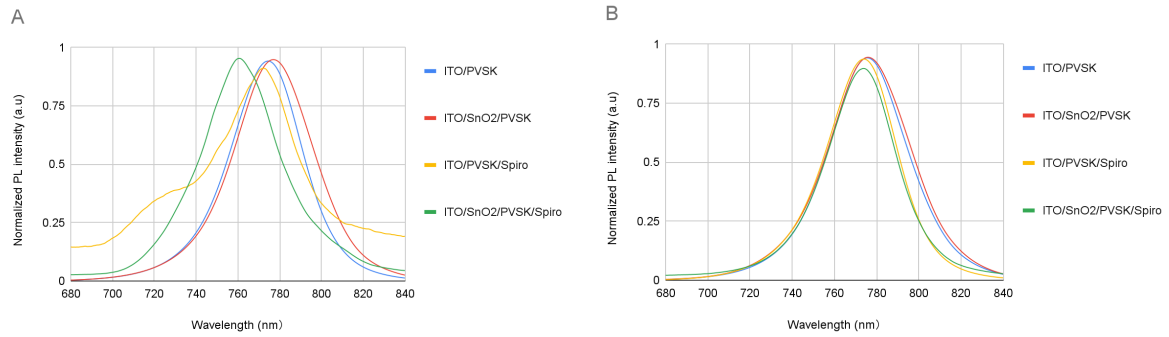

Fig.3.5 A) PL spectra of samples with ratio 0f 0.9, B) PL spectra of samples with ratio of 1.0.

3.3 Scanning Kelvin Probe characterization

Fig. 3.6 represents the samples with a ratio of 0.9 for MAI/PbI_2. Each figure has four graphs, each graph represents a different CTL of perovskite solar cells, Fig. 3.6A is ITO/PVSK, Fig. 3.6B is ITO/PVSK/Spiro, and Fig. 3.6C is ITO/SnO_2/PVSK, and Fig. 3.6D is ITO/SnO_2/PVSK/Spiro. Each graph consists of how the work function of solar cells changes in the dark and under illumination with a switching on/off period of 200s and a degradation period of 2 years. The blue curves represent the results measured under the illumination from Solar Simulator and the red curves represent the results measured under the illumination from Halogen Lamp. In the graph we can also see the photovoltaic

effect (photovoltage), which is the difference between WF in the dark and under the light. Photovoltage was calculated by equation (2). It represents the energy generated by the light. In this discussion, we will compare our results only to the results on day 28 in the article [2], because they are the closest result in terms of time. The measurements in the article [2] were done two years ago.

$$PV = WF_{light} - WF_{dark} \quad (2)$$

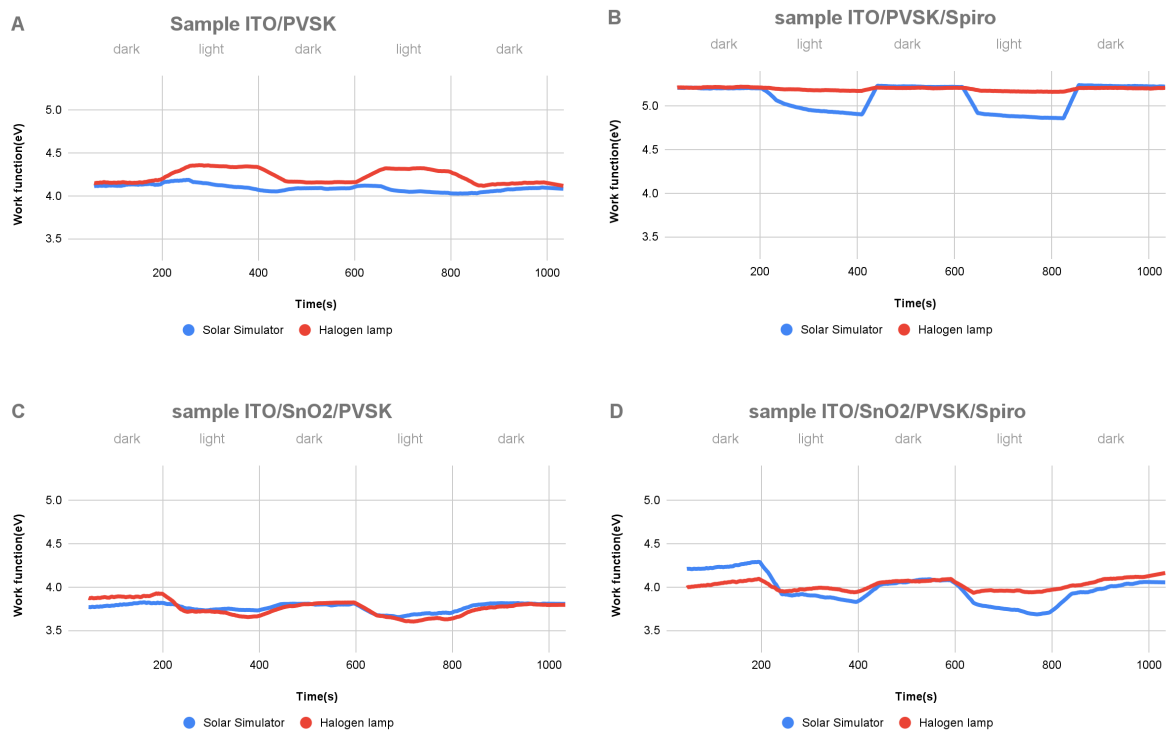

Fig. 3.6 Kelvin Probe study of degradation for MAI/PbI_2=0.9.

In Fig. 3.6A, the curves of the two sets of data are quite different. The Solar Simulator (blue) line is very unstable, while the Halogen lamp (red) line is relatively stable. The photovoltage on both sides are also quite different, but both illustrate a negative PV. The Halogen lamp (red) line has a very good photovoltaic of -0.21 V. The county has only about -0.07 V PV, but it is very unstable and fluctuating. The negative PV means that electrons were not extracted to the bottom electrode but rather diffused to the PVSK surface. Compared with the data two years ago, the Solar Simulator (blue) and Halogen lamp (red) trend have decreased from the original 4.96 ± 0.03 eV to about 4.09 ± 0.06 eV and 4.04 ± 0.03 eV in the dark, which has a decrease of 0.87 ± 0.09 eV and 0.92 ± 0.06 eV, respectively.

Looking at Fig. 3.6B we could see that the WFs for both light sources were almost equal Solar simulator (blue) 5.21 ± 0.02 eV and Halogen lamp (red) 5.2 ± 0.1 eV. There are significant differences in the sample PV where PV under the Solar Simulator (blue) is 0.3 V and under the

Halogen lamp (red) is 0.03 V. The reason might be that Solar Simulator (blue) light (light emittation 400-1100 nm) has wider spectral range then Halogen lamp (red) light (light emittation 380-750 nm). The different layers of the sample absorb different light ranges [28]. The samples are better at absorbing the light from the Solar Simulator. Nevertheless, it is more stable than the ITO/PVSK sample in figure A. WF has decreased by 0.07 ± 0.04 eV under light from a Solar simulator (blue) and WF has relatively decreased by 0.08 ± 0.03 eV under light from a Halogen lamp (red). In addition, PV has decreased by 0.97 V for Halogen lamps, but it has risen by 0.2 V for Solar Simulator compared to the old data [2]. We expected that PV would decrease, so it is interesting that we are getting an increase in PV for Solar Simulator. Solar simulators have a wider range of excitation wavelengths.

Furthermore, the curves from Fig. 3.6C looks unstable. The PV of the Solar Simulator (blue) line remains around 0.08 V and the Halogen lamp (red) line is 0.27 V. Compared with the results from 2 years ago, it has decreased by 0.50 ± 0.10 V for Solar Simulator and 0.73 ± 0.12 V for the Halogen lamp. One more thing to be discovered is there is a shift in charge during the illumination. The reason is we observed a negative PV in the 2 years old results (-17 V)[2], but we observe a positive PV now. Positive PV means that the electrons were extracted by the ETL, so holes were distributed to the surface. This sample became more transparent during the storage time and PL spectra were shifted which could be related to the change of the PV orientation.

In Fig. 3.6D we can see that the Halogen lamp (red line) has a very bad result. PV for the Halogen lamp (red) trend has around 0.18 V, which is very different from the Solar Simulator (blue) trend. The Solar Simulator (blue) line has a PV of 0.44 V, but both of them are very unstable and fluctuating, it seems that it is not a suitable sample, definitely not suitable for mass production in the future. An interesting phenomenon is that we can find the graphs of Fig. 3.6C and Fig. 3.6D are very similar. From the composition of their materials, we can see that Figure 3.6D only has one more component of SnO_2 compared to Fig. 3.6C. The response of the two samples to the illuminance can be said to have a fundamental change. Fig. 3.6D has a higher WF under the illumination of a Solar Simulator (blue), and figure C has a higher WF under the illumination of a Halogen lamp (red). In this Fig. 3.6D, we can find that WF has decreased by about 0.89 ± 0.17 eV for Solar Simulator and 1.04 ± 0.12 eV compared with the two year old data [2]. The decrease of the WF could be related to aging of the sample. The changes were also observed in the visual image (transparency of the sample).

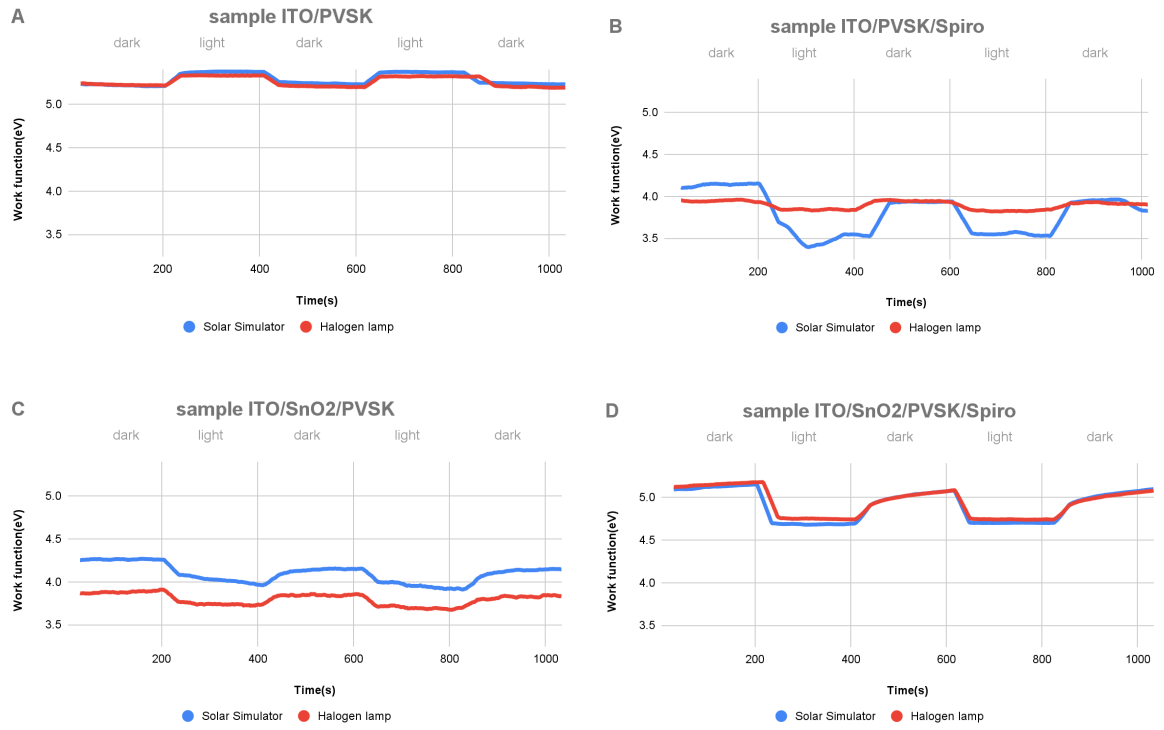

Fig. 3.7 Kelvin Probe study of degradation for MAI/PbI_2=1.0.

In Fig. 3.7, we can see the graphs for PVSK samples with ratios MAI/PbI_2=1.0. Again there are four different images where Fig. 3.7A represents ITO/PVSK, Fig. 3.7B represents ITO/PVSK/Spiro, Fig. 3.7C represents ITO/SnO_2/PVSK and Fig. 3.7D represents ITO/SnO_2/PVSK/Spiro. In Fig. 3.7A, we could see that both trends Solar Simulator (blue) and Halogen lamp (red) are similar with a slightly higher WF of the Solar Simulator (blue) than the Halogen (red) trend. WF fluctuated between 5.23 ± 0.02 eV and 5.21 ± 0.03 eV in the dark and 5.38 ± 0.01 eV and 5.32 ± 0.01 eV under the light, respectively. In addition, they have a decrease of WF for 0.53 ± 0.12 eV and 0.51 ± 0.13 eV, respectively. Although the decrease in the WF was only around 0.5 eV, the PV had a greater drop, from the initial -0.8 V from 2 years ago [2] to -0.16 V for the Solar Simulator (blue) and -0.11 V for the Halogen lamp (red).

In Fig. 3.7B, we can see that it has different responses to the different illumination sources, and the response to the Halogen lamp (red) is very low. The photovoltage of the Solar Simulator is about 0.8 V, but the Halogen lamp is about 0.1 V. The positive PV means that holes were extracted by Spiro. Compared with two years ago, the WF has decreased by nearly 1.07 ± 0.31 eV for the Solar Simulator and 1.13 ± 0.09 eV for the Halogen lamp, which is very high compared to the rest of the results that we have computed.

Moreover, the trends in Fig. 3.7C are very similar to the trends for sample ITO/PVSK/Spiro in Fig. 3.7B. The Solar Simulator (blue) trend has a higher WF than the Halogen lamp (red) trend, they have 4.2 ± 0.04 eV and 3.85 ± 0.05 eV, respectively. They have a similar trend and WF compared to

the Halogen lamp (red) trend in Fig. 3.7B. However, they also have different values for PV, they have 0.26 V and 0.28 V, respectively. The WF under the light from the Solar Simulator decreased by 0.51 ± 0.07 eV and under the Halogen lamp decreased by 0.86 ± 0.08 eV compared to results in the work Kuliček et. al. [2]. Also compare the results in the work of Kulicek et. al. [2] we observed the same positive PV. Two years ago it was negative, but we observe positive PV now. It means that ETL collects the electrons and holes are spread to the sample surface.

The last graph in Fig. 3.7D shows two trends that are highly overlapping. The WF is 5.07 ± 0.06 eV for the Solar Simulator (blue) line and 5.08 ± 0.07 eV for the Halogen lamp (red) line. There is a decrease of the WF around 0.05 ± 0.12 eV for the Solar Simulator (blue) trend and 0.06 ± 0.13 eV for the Halogen (red) trend compared to the results in the [2]. Also, the signal under the Solar simulator (blue) light and the signal under the Halogen lamp (red) light have a very approximate PV, Solar simulators 0.43 V and 0.4 V for the Halogen lamp. If we compare the results from 2 years ago, there is only a 0.2 V difference in PV. There are slight changes in the PV and WF of ITO/SnO_2/PVSK/Spiro after the two years.

Also there is possibility that ITO glass can influence the WF and PV, mostly in the case of the samples ITO/PVSK/Spiro and ITO/SnO_2/PVSK/Spiro because of their transparency. ITO is a conductive-optical material. ITO glass interferes with the incoming UV light, partially absorbing a significant amount of photons and thus undergoing electronic excitations [29]. So we decided to measure the surface potential in the dark and under illumination of the pure ITO glass used for deposition on the PVSK in this thesis.

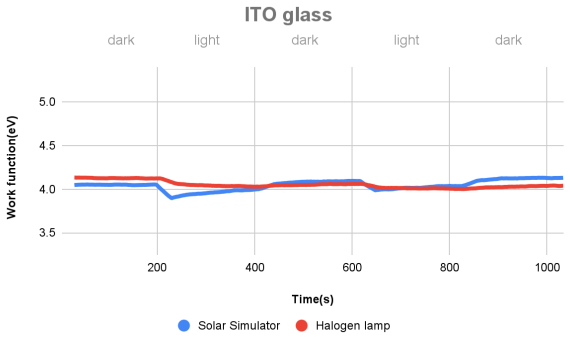

Fig. 3.8 Work function in the dark and under illumination on ITO glass.

Fig. 3.8 illustrates the WF of ITO glass under the illumination of the Solar Simulator (blue) and Halogen lamp (red). The WF of the ITO glass under the Solar Simulator (blue) was 4.2 ± 0.1 eV and under the light for the Halogen lamp was 4.1 ± 0.1 eV. The results showed that PV of ITO under light from a Halogen lamp (red) had a poor response but significant response under the light from Solar Simulator (blue). As was mentioned above ITO is an electro-optical material and due to the degradation of our samples (some samples become transparent after two years), ITO could be more exposed to the light. Illumination of ITO glass caused absorption of the photons and excitation of

electrons which could influence the final signal from our samples. By comparison of the WF results of ITO and samples used in this thesis we can conclude that influence of the ITO glass to the WF and the PV of the samples are small. The changes in the WF and PV were probably caused by the changes in the layer stack of the samples during the storage time. The different reaction of samples illuminated by the two different light sources could be explained by the different wavelength range of the sources because the layers/materials used in the preparation of the samples have a different light absorption range [17].

At the moment, we cannot say more about material chemical changes during the storage time because these changes also have an influence on the final opto-electronic properties. It probably is the formation of some salts, but we need to do more experiments to explain the changes in material composition and properties, for example, Raman spectroscopy, Fourier-transform infrared spectroscopy (FTIR), and X-ray photoelectron spectroscopy (XPS).

4. Conclusion

In this thesis, we observed the changes in morphology and aging of perovskite solar cells with different CTLs and ratios of MAI/PbI_2 after two years through the methods AFM, Scanning Kelvin Probe in the dark and under the illumination, and Confocal Photoluminescence Micro-spectroscopy. The sample photographs show the changes under different CTLs combinations and different ratios of MAI/PbI_2. After two years, the most significant change is that the perovskite samples with Spiro's deposition will increase their transparency, especially with a lower MAI ratio.

The AFM topography images illustrate the changes on surface properties of the perovskite with different CTLs and the ratio of MAI/PbI_2, such as grain size and roughness. Among the observed CTLs, changes in the photovoltage and work function on the all samples also suggest possible structural differences in the PVSK layers that AFM on the surface cannot directly observe. In the Kelvin Probe study the changes in the WF and PV were observed in the comparison to the old data. PL maps showed the differences in the morphology of perovskite samples in the both ratios of the MAI/PbI_2. The most significant difference was in samples with the full layer stack ITO/SnO_2/PVSK/Spiro. The ITO/SnO_2/PVSK/Spiro with the ratio of MAI/PbI_2= 0.9 had smaller features while samples with the ratio of MAI/PbI_2= 1.0 showed bigger features. PL maps correlated with the AFM morphology. The PL spectra for samples with the Spiro layer for the MAI/PbI_2 ratio of 0.9 showed the left-shifts related to the transparency of the samples as well as the changes of the layer stack during the storage.

Significant changes were shown in the PV for ITO/SnO_2/PVSK sample for the both studied ratios of the MAI/PbI_2. The PV was positive compared to negative PV measured two years ago. The changes in the WF and PV are related to the changes in the layer stack during the two years storage time. Also in this thesis we compared the WF and PV from two sources of the light Solar simulator (blue) and the Halogen lamp (red). The differences in the WF are present as well as in the PV values. The most significant difference in the PV values were observed for the ITO/PVSK and ITO/PVSK/Spiro of the MAI/PbI_2= 0.9; and ITO/PVSK/Spiro and ITO/SnO_2/PVSK of the ratio MAI/PbI_2= 1.0, where the PV values obtained under the Solar Simulator light was higher the the PV values obtained under the light of Halogen lamp. We did the characterization of pure ITO glass by the Kelvin Probe in the dark and under the illumination. And concluded that the influence of the ITO glass to the WF and PV values are minimal. The changes in the WF and PV mostly are related to the

changes in the layer stack during the two years storage time as well as the excitation wavelength range of the light sources.

The studied perovskite materials showed the opto-electronics reactions after two years of storage and the effect of aging was reflected in their opto-electronic properties.

References

[1] A. Abudulimu, L. Liu, G. Liu, N. Aimaiti, B. Rezek, Q. Chen, Crucial role of charge transporting layers on ion migration in perovskite solar cells, Journal of Energy Chemistry. 47 (2020) 132–137. https://doi.org/10.1016/j.jechem.2019.12.002.

[2] J. Kuliček, A. Abuduliimu, L. Lang, L. Guilin, Q. Chen, B. Rezek, MICROSCOPIC AND KELVIN PROBE STUDY OF CHARGE TRANSPORTING LAYERS ROLE IN MAPI PEROVSKITES WITH VARIED COMPOSITION, in: 2020: pp. 130–135. https://doi.org/10.37904/nanocon.2019.8662.

[3] W.-J. Yin, T. Shi, Y. Yan, Unique Properties of Halide Perovskites as Possible Origins of the Superior Solar Cell Performance, Advanced Materials. 26 (2014) 4653–4658. https://doi.org/10.1002/adma.201306281.

[4] F. Gao, Y. Zhao, X. Zhang, J. You, Recent Progresses on Defect Passivation toward Efficient Perovskite Solar Cells, Adv. Energy Mater. 10 (2020) 1902650. https://doi.org/10.1002/aenm.201902650.

[5] H. Pan, X. Zhao, X. Gong, H. Li, N.H. Ladi, X.L. Zhang, W. Huang, S. Ahmad, L. Ding, Y. Shen, M. Wang, Y. Fu, Advances in design engineering and merits of electron transporting layers in perovskite solar cells, Mater. Horiz. 7 (2020) 2276–2291. https://doi.org/10.1039/D0MH00586J.

[6] S. Razza, S. Castro-Hermosa, A. Di Carlo, T.M. Brown, Research Update: Large-area deposition, coating, printing, and processing techniques for the upscaling of perovskite solar cell technology, APL Materials. 4 (2016) 091508. https://doi.org/10.1063/1.4962478.

[7] S.N.R. Kantareddy, I. Mathews, S. Sun, M. Layurova, J. Thapa, J.-P. Correa-Baena, R. Bhattacharyya, T. Buonassisi, S.E. Sarma, I.M. Peters, Perovskite PV-Powered RFID: Enabling Low-Cost Self-Powered IoT Sensors, IEEE Sensors Journal. 20 (2020) 471–478. https://doi.org/10.1109/JSEN.2019.2939293.

[8] F. Giustino, H.J. Snaith, Toward Lead-Free Perovskite Solar Cells, ACS Energy Lett. 1 (2016) 1233–1240. https://doi.org/10.1021/acsenergylett.6b00499.

[9] P.V. Kamat, J. Bisquert, J. Buriak, Lead-Free Perovskite Solar Cells, ACS Energy Lett. 2 (2017) 904–905. https://doi.org/10.1021/acsenergylett.7b00246.

[10] X. Meng, Y. Wang, J. Lin, X. Liu, X. He, J. Barbaud, T. Wu, T. Noda, X. Yang, L. Han, Surface-Controlled Oriented Growth of FASnI3 Crystals for Efficient Lead-free Perovskite Solar Cells, Joule. 4 (2020) 902–912. https://doi.org/10.1016/j.joule.2020.03.007.

[11] T. Wu, X. Liu, X. Luo, X. Lin, D. Cui, Y. Wang, H. Segawa, Y. Zhang, L. Han, Lead-free tin perovskite solar cells, Joule. 5 (2021) 863–886. https://doi.org/10.1016/j.joule.2021.03.001.

[12] A. Mahapatra, D. Prochowicz, M.M. Tavakoli, S. Trivedi, P. Kumar, P. Yadav, A review of aspects of additive engineering in perovskite solar cells, J. Mater. Chem. A. 8 (2019) 27–54. https://doi.org/10.1039/C9TA07657C.

[13] D. Yue, F. You, S.B. Darling, Domestic and overseas manufacturing scenarios of silicon-based photovoltaics: Life cycle energy and environmental comparative analysis, Solar Energy. 105 (2014) 669–678. https://doi.org/10.1016/j.solener.2014.04.008.

[14] J.K.W. Ho, H. Yin, S.K. So, From 33% to 57% – an elevated potential of efficiency limit for indoor photovoltaics, J. Mater. Chem. A. 8 (2020) 1717–1723. https://doi.org/10.1039/C9TA11894B.

[15] F.H. Alharbi, S. Kais, Theoretical limits of photovoltaics efficiency and possible improvements by intuitive approaches learned from photosynthesis and quantum coherence, Renewable and Sustainable Energy Reviews. 43 (2015) 1073–1089. https://doi.org/10.1016/j.rser.2014.11.101.

[16] Y. Shao, Y. Fang, T. Li, Q. Wang, Q. Dong, Y. Deng, Y. Yuan, H. Wei, M. Wang, A. Gruverman, J. Shield, J. Huang, Grain boundary dominated ion migration in polycrystalline organic–inorganic halide perovskite films, Energy Environ. Sci. 9 (2016)

1752–1759. https://doi.org/10.1039/C6EE00413J.
[17] Y. Lin, B. Chen, Y. Fang, J. Zhao, C. Bao, Z. Yu, Y. Deng, P.N. Rudd, Y. Yan, Y. Yuan, J. Huang, Excess charge-carrier induced instability of hybrid perovskites, Nature Communications. 9 (2018). https://doi.org/10.1038/s41467-018-07438-w.
[18] B. Hailegnaw, S. Kirmayer, E. Edri, G. Hodes, D. Cahen, Rain on Methylammonium Lead Iodide Based Perovskites: Possible Environmental Effects of Perovskite Solar Cells, J. Phys. Chem. Lett. 6 (2015) 1543–1547. https://doi.org/10.1021/acs.jpclett.5b00504.
[19] D. O'Connor, D. Hou, Manage the environmental risks of perovskites, One Earth. 4 (2021) 1534–1537. https://doi.org/10.1016/j.oneear.2021.11.002.
[20] Y. Nishigaki, T. Nagai, M. Nishiwaki, T. Aizawa, M. Kozawa, K. Hanzawa, Y. Kato, H. Sai, H. Hiramatsu, H. Hosono, H. Fujiwara, Extraordinary Strong Band-Edge Absorption in Distorted Chalcogenide Perovskites, Solar RRL. 4 (2020) 1900555. https://doi.org/10.1002/solr.201900555.
[21] S. Wang, Y. Jiang, E.J. Juarez-Perez, L.K. Ono, Y. Qi, Accelerated degradation of methylammonium lead iodide perovskites induced by exposure to iodine vapour, Nat Energy. 2 (2016) 1–8. https://doi.org/10.1038/nenergy.2016.195.
[22] K.O. Ogunniran, N.T. Martins, Humidity and Moisture Degradation of Perovskite Material in Solar Cells: Effects on Efficiency, IOP Conf. Ser.: Earth Environ. Sci. 655 (2021) 012049. https://doi.org/10.1088/1755-1315/655/1/012049.
[23] M. Adil Afroz, N. Ghimire, K.M. Reza, B. Bahrami, R.S. Bobba, A. Gurung, A.H. Chowdhury, P.K. Iyer, Q. Qiao, Thermal Stability and Performance Enhancement of Perovskite Solar Cells Through Oxalic Acid-Induced Perovskite Formation, ACS Appl. Energy Mater. 3 (2020) 2432–2439. https://doi.org/10.1021/acsaem.9b02111.
[24] APS04-N2-RH – KP Technology, (n.d.). https://www.kelvinprobe.com/product/aps04-n2-rh/ (accessed May 11, 2022).
[25] Atomic Force Microscopy (AFM) - WITec Raman Imaging, Oxford Instruments. (n.d.). https://raman.oxinst.com/techniques/scanning-probe-microscopy (accessed May 8, 2022).
[26] Schott_KL_1500HAL_UserManual_LAMBDA.pdf, (n.d.). https://www.lambdaphoto.co.uk/pdfs/Schott/Schott_KL_1500HAL_UserManual_LAMBDA.pdf (accessed May 11, 2022).
[27] Light absorption and photoluminescence (PL) spectroscopy, Chemistry LibreTexts. (2019). https://chem.libretexts.org/Courses/Franklin_and_Marshall_College/Introduction_to_Materials_Characterization__CHM_412_Collaborative_Text/Spectroscopy/Light_absorption_and_photoluminescence_(PL)_spectroscopy (accessed May 12, 2022).
[28] L. Yue, B. Yan, M. Attridge, Z. Wang, Light absorption in perovskite solar cell: Fundamentals and plasmonic enhancement of infrared band absorption, Solar Energy. 124 (2016) 143–152. https://doi.org/10.1016/j.solener.2015.11.028.
[29] M. Thirumoorthi, J. Thomas Joseph Prakash, Structure, optical and electrical properties of indium tin oxide ultra thin films prepared by jet nebulizer spray pyrolysis technique, Journal of Asian Ceramic Societies. 4 (2016) 124–132. https://doi.org/10.1016/j.jascer.2016.01.001.